

Orthogonal polarization mode phenomenon in pulsars

R. T. Gangadhara

Max-Planck-Institut für Radioastronomie, Auf dem Hügel 69, D-53121 Bonn, Germany
ganga@mpifr-bonn.mpg.de

Received 14 October 1996/ Accepted 2 June 1997

Abstract. We consider the polarization properties of radiation emitted by relativistic charged particles while moving along the curved magnetic field lines in a pulsar magnetosphere. We propose that the radiation emitted by positrons and electrons while moving along the curved magnetic field lines is orthogonally polarized. The polarization angle of each orthogonal polarization mode is well described by the rotating vector model. However, the polarization angle swings observed in micropulses and sub-pulses are often found to be contrary to the rotating vector model, and such swings are expected to arise due to the coherent superposition of orthogonal polarization modes.

As an application of our model, we discuss the polarization of pulsar PSR B0950+08 at the frequency 1.71 GHz. Data on individual pulses, obtained using the 100-m Effelsberg radiotelescope, was statistically analysed and the results are presented as probability of occurrence gray-scale plots. We find that pulsars emit radiation mainly in the form of two independent orthogonal modes. It seems, they exist at all pulse longitudes but at some longitudes one mode dominates over the other. The polarization angle gray-plot indicates two most favoured angles separated by approximately 90° at each pulse longitude. The depolarization is mainly caused by the incoherent superposition of orthogonal modes.

We infer from this study that pulsar radiation consists of two major elliptically polarized electromagnetic waves with orthogonal polarization angles. Our model predicts that such waves could be radiated by the positrons and the electrons accelerated along the curved magnetic field lines. The sense of circular polarization of these modes depend upon from which side of particle trajectory the radiation is received.

Key words: Pulsars: individual: PSR B0950+08—radiation mechanism: non-thermal

1. Introduction

Pulsar radio emission and further propagation effects in the magnetosphere are not well understood. This situation is partly due to the difficulty in understanding particle acceleration and current flow in pulsars superstrong magnetic field. From the observation point of view curvature radiation seems to be most attractive among all the proposed radio emission mechanisms (Michel 1991; Mészáros 1992; Xilouris et al. 1994). However the coherent curvature emission by bunches has been often criticized (e.g. Melrose 1981). Curvature radiation is quite similar to synchrotron radiation, with the only difference that the role of Larmor radius is played here by the radius of curvature of magnetic field lines. Michel (1987a) has indicated that curvature radiation has significant circular polarization when viewed at an angle to the plane of a magnetic field line, and reverses sense when viewed from the other side.

The curvature radiation model has been developed by assuming that particles follow the curved field lines (Sturrock 1971; Ruderman & Sutherland 1975). The theory of synchrotron radiation is developed by assuming uniform and straight field lines while the curvature radiation is developed by ignoring the spiral motion of the particles. The most often cited reason for ignoring spiral motion is that particles will instantly lose the energy associated with perpendicular component of motion by synchrotron radiation, cascading down to zero free energy. This is true near the polar cap where the field lines are straight. But when the particles move into the curved region of field lines they recover the perpendicular component of momentum as the field lines curve off from the direction of particle velocity. Hence the radiation emitted by charged particles while moving along the curved magnetic field lines cannot be described by considering either synchrotron or simple curvature radiation separately. Gil & Snakowski (1990) have attempted to examine the polarization properties of curvature radiation but they have also not considered the role of magnetic force.

One of the most fascinating features of pulsar radiation is the occurrence of orthogonal polarization modes (OPM), i.e., the two electromagnetic waves with orthogonal electric vectors. This phenomenon has become difficult to explain by emission models based on the simple curvature emission, as it cannot specify the two preferred polarization angles. There are other models based on the propagation effects but one would expect such effects to be strongly dependent on frequency and require special viewing angles (Michel 1991), whereas observations indicate the phenomenon is broad band. The interpretation based on the geometrical effects (Michel 1987b) indicates that two modes could be due to the overlap of radiation from two distinct emission regions in the magnetosphere. However, it is not clear why the two separated sources have nearly orthogonal polarization.

Pulsars have been noted for their highly polarized radiation. To understand the phenomenology of pulsar polarization, many attempts have been made to fit the average polarization angle swing within the context of the rotating vector model (RVM) (Radhakrishnan & Cooke 1969). However many pulsars do not fit with this interpretation (Manchester 1971; Rankin et al. 1974) and such discrepancies have been attributed to the occurrence of OPM (Backer et al. 1976; Gil & Lyne 1995). The relative strengths of OPM vary with pulse longitude, thus causing discontinuities in the average pulse polarization angle swing (Cordes & Hankins 1977). The switching between OPM mostly but not always occurs on the boundaries of micropulses and subpulses (Cordes & Hankins 1977), and may be intrinsic to the emission process (Manchester et al. 1975; Cordes et al. 1978). The single-pulse studies (Stinebring et al. 1984a,b) show that OPM overlap, and in the vicinity of pulse longitude where jump occurs some pulses prefer to have one polarization and some have other polarization. All these fine details are lost when the pulses are averaged. The depolarization in average pulse occurs due to the superposition of OPM (Lyne et al. 1971; Manchester et al. 1975; Stinebring et al. 1984a).

Cordes et al. (1978) have reported the existence of OPM with opposite senses of circular polarization in pulsar PSR B2020+28 at 430 MHz. They found no evidence for a threshold intensity in the occurrence of OPM. The peak subpulse emission can be in either OPM, and sometimes transitions between modes do not occur on the edges of subpulses. Therefore, the occurrence of OPM may be stochastic and perhaps indicating the untenability of a geometric interpretation of the transitions as aspects of an angular beam of radiation.

The motion of a charged particle along a rotating magnetic field line is discussed by Gangadhara (1995; 1996a) and in the case of a curved magnetic field line (Gangadhara 1996b), and the studies indicated that OPM may be produced by positrons and electrons, as they have got opposite senses of gyration. In this paper, we show that the relativistic positrons and electrons can produce OPM be-

cause while moving along a curved magnetic field line their accelerations become inclined with respect to the radius of curvature of a field line. We propose the coherent superposition of OPM as a physical explanation for the polarization angle swings observed in micropulses and subpulses. In Sect. 2 we discuss the forces acting on a positron and an electron while moving along a curved magnetic field line. The radiation fields due to a positron and an electron are derived in Sect. 3. The polarization properties of radiation fields are computed in Sect. 4. Finally, in Sect. 5, we present a series of gray-plots describing the polarization states of OPM from PSR B0950+08, and discuss the possible explanation based on our model.

2. Motion of relativistic charged particles along curved magnetic field lines

In the physics of pulsar magnetosphere, a very important question is how are the charged particles ejected from the surface of a neutron star, and it has been discussed by many authors (e.g. Herring & Nichols 1949; Good & Müller 1956; Ruderman & Sutherland 1975; Kundt & Schaaf 1993). If particles are produced with the velocity having a component perpendicular to the magnetic field they quickly radiate away the energy associated with that component of motion by synchrotron radiation. Hence the particle gyration becomes almost absent near the polar cap. Once the particles radiate away the energy associated with the perpendicular component of velocity, they are free to move along the field lines as long as they are straight. But when the particles enter the curved region of field lines, they recover perpendicular component of velocity at the expense of parallel component (Gangadhara 1996b) as the field line curves off from the direction of particle motion (Fig. 1). This phenomenon must be true for both primary as well as secondary particles.

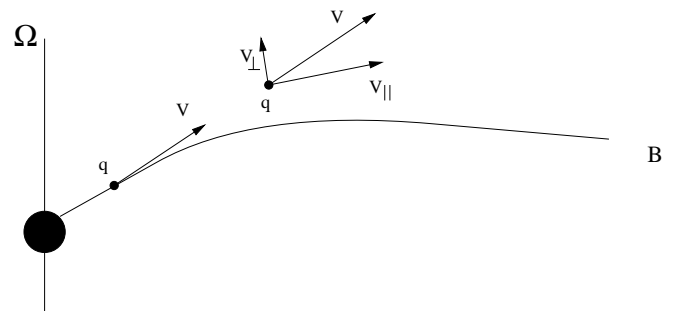


Fig. 1. Motion of a particle with charge q and velocity \mathbf{v} along a curved field line \mathbf{B} .

The motion of a particle along a curved magnetic field line is governed mainly by the magnetic Lorentz force \mathbf{F}_B and the centrifugal (inertial) force \mathbf{F}_c . Figure 2 shows the

directions of these forces when a positron and an electron are in motion along a curved magnetic field line. The net force acting on a particle is given by

$$\mathbf{F}_i = \mathbf{F}_{ci} + \mathbf{F}_{Bi}, \quad (1)$$

where $i = p$ for a positron and e for an electron. The magnetic force is

$$\mathbf{F}_{Bi} = \frac{q_i}{c} \mathbf{v}_{\perp i} \times \mathbf{B} \quad (2)$$

and the centrifugal force is

$$\mathbf{F}_{ci} = \frac{\gamma_i m_i v_{\parallel i}^2}{\rho^2} \boldsymbol{\rho}, \quad (3)$$

where m_i and q_i are the mass and charge, γ_i is the relativistic Lorentz factor, $v_{\parallel i}$ and $v_{\perp i}$ are the components of velocity with respect to the magnetic field \mathbf{B} , respectively. Here $\boldsymbol{\rho}$ is the radius of curvature of a magnetic field line.

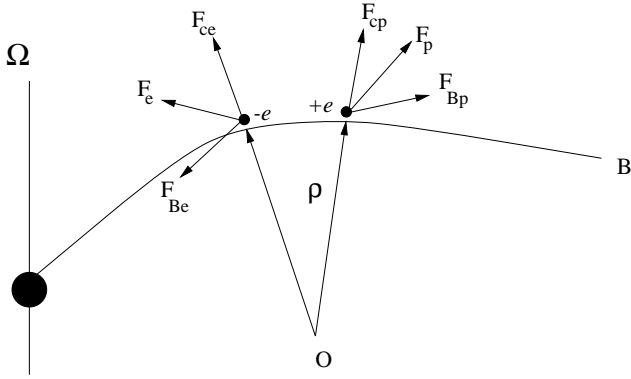


Fig. 2. The forces \mathbf{F}_{Bp} and \mathbf{F}_{cp} act on a positron, and \mathbf{F}_{Be} and \mathbf{F}_{ce} act on an electron while they are in motion along a curved field line \mathbf{B} . Here ρ is the radius of curvature of field line.

Initially, magnetic and centrifugal forces act in the directions perpendicular and parallel to the plane of magnetic field line, respectively. The motion of particles along curved field lines is discussed by Jackson (1976) and Gangadhara (1996b). The gyration motion (spiral motion) is considered as the zero-order-motion, and the motion that arises due to the curvature of field lines as the first-order motion. In the absence of initial perpendicular component of velocity, particles cannot gyrate around the curved magnetic field lines. The reason is that as particle attempts to spiral, field line curves off to the side and hence the centrifugal force prevents it from spiraling (Gangadhara 1995; 1996a). Also, it is observationally known that no generalized Faraday rotation is evident in pulsar magnetospheres (Cordes 1983; Lyne & Smith 1990). There is *no central force* at O, and the magnetic force plays the role of

centripetal force to keep the particle on track. But the peculiarity of magnetic force is that it acts in the directions perpendicular to the magnetic field and not always in the direction of radius of curvature. *Since* $|\mathbf{F}_{Bi}| \approx |\mathbf{F}_{ci}|$, *the net forces* \mathbf{F}_p *and* \mathbf{F}_e *are inclined through, respectively, $\sim 45^\circ$ and -45° with respect to the plane of magnetic field line.* Therefore, the net accelerations of positrons and electrons become orthogonal in the curved magnetic field lines of pulsar magnetosphere. The detailed computation of particle dynamics, including radiation reaction, is under consideration and published elsewhere.

3. Radiation fields of positrons and electrons accelerated in curved magnetic field lines

Consider a relativistic particle with charge q moving along a curved trajectory C (space curve) in the xyz -coordinate system (Fig. 3). Let θ be the angle between particle position \mathbf{r} and yz -plane. A distant observer at P receives radiation at an angle ϕ_p from the plane of particle orbit. The electric field of radiation at the observation point is given by (Jackson 1976)

$$\mathbf{E}(\mathbf{r}, t) = \frac{q}{c} \left[\frac{\hat{k} \times [(\hat{k} - \boldsymbol{\beta}) \times \dot{\boldsymbol{\beta}}]}{S \sigma^3} \right]_{\text{ret}}, \quad (4)$$

where $\sigma = 1 - \boldsymbol{\beta} \cdot \hat{k}$. The distance from radiating region to the observer is S , the propagation vector is \hat{k} , and the velocity and acceleration of particle are $\boldsymbol{\beta} = \mathbf{v}/c$ and $\dot{\boldsymbol{\beta}}$.

The radiation emitted by a relativistic charged particle has a broad spectrum. The range of frequency spectrum is estimated by taking Fourier transformation of electric field of radiation:

$$\mathbf{E}(\omega) = \frac{1}{\sqrt{2\pi}} \int_{-\infty}^{+\infty} \mathbf{E}(t) e^{i\omega t} dt. \quad (5)$$

In Eq. (4), *ret* means evaluated at the retarded time $t' + \frac{S(t')}{c} = t$. By changing the variable of integration from t to t' , we obtain

$$\mathbf{E}(\omega) = \frac{1}{\sqrt{2\pi}} \frac{q}{c} \int_{-\infty}^{+\infty} \frac{\hat{k} \times [(\hat{k} - \boldsymbol{\beta}) \times \dot{\boldsymbol{\beta}}]}{S \sigma^2} e^{i\omega\{t'+S(t')/c\}} dt', \quad (6)$$

where we have used $dt = \sigma dt'$.

When the observation point is far away from the region of space where the acceleration occurs, the propagation vector \hat{k} can be taken constant in time. Furthermore the distance $S(t')$ can be approximated as

$$S(t') \approx S_0 - \hat{k} \cdot \mathbf{r}(t'), \quad (7)$$

where S_o is the distance between the origin O and the observation point P, and $\mathbf{r}(t')$ is the position of particle relative to O. Then Eq. (6) becomes

$$\mathbf{E}(\omega) \approx \frac{q e^{i\omega S_o/c}}{\sqrt{2\pi S_o c}} \int_{-\infty}^{+\infty} \frac{\hat{k} \times [(\hat{k} - \boldsymbol{\beta}) \times \dot{\boldsymbol{\beta}}]}{\sigma^2} e^{i\omega\{t - \hat{k} \cdot \mathbf{r}/c\}} dt, \quad (8)$$

where the primes on the time variable have been omitted for brevity. The integrand in Eq. (8), excluding exponential, is a perfect differential, therefore, we can integrate by parts, and obtain

$$\mathbf{E}(\omega) = -i \frac{q\omega e^{i\omega S_o/c}}{\sqrt{2\pi S_o c}} \int_{-\infty}^{+\infty} \hat{k} \times (\hat{k} \times \boldsymbol{\beta}) e^{i\omega\{t - \hat{k} \cdot \mathbf{r}/c\}} dt. \quad (9)$$

The polarization of emitted radiation can be estimated for a specified motion with known $\mathbf{r}(t)$ and $\boldsymbol{\beta}$.

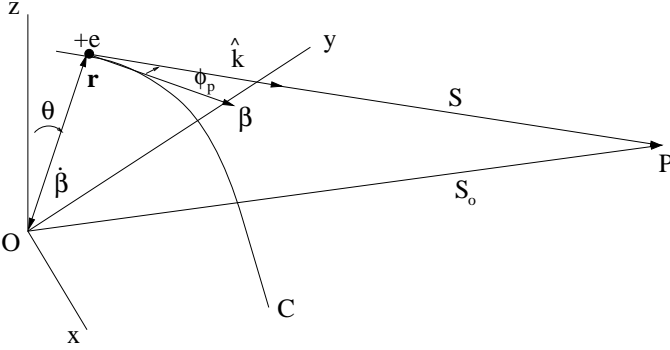


Fig. 3. The geometry used to describe the radiation emitted by a positron while moving along a curved trajectory C. Here θ is the angle between yz-plane and \mathbf{r} , and ϕ_p is the angle between $\boldsymbol{\beta}$ and \hat{k} .

3.1. Radiation field due to a positron

Since the duration of pulse $\Delta t \sim R/c\gamma$ is very short, it is necessary to know the position $\mathbf{r}(t)$ and velocity $\boldsymbol{\beta}$ of particle over only small arc of the trajectory whose tangents are in the general direction of observation. Therefore, for a positron moving under the action of magnetic and centrifugal forces, we take:

$$\mathbf{r}(t) = R \left(\sin \theta, \frac{\cos \theta}{\sqrt{2}}, \frac{\cos \theta}{\sqrt{2}} \right), \quad (10)$$

$$\boldsymbol{\beta}(t) = \beta \left(\cos \theta, -\frac{\sin \theta}{\sqrt{2}}, -\frac{\sin \theta}{\sqrt{2}} \right). \quad (11)$$

Since the integral in Eq. (9) has to be computed over the path of particle, the unit vector \hat{k} can be chosen, without

loss of generality, to lie in a plane which is parallel to the xy-plane:

$$\hat{k} = (\cos \phi_p, \sin \phi_p, 0), \quad (12)$$

where ϕ_p is the angle made by \hat{k} with respect to the positron velocity. Using Eqs. (11) and (12), the vector part of the integrand in Eq. (9) can be written as

$$\hat{k} \times (\hat{k} \times \boldsymbol{\beta}) = \beta \left[\frac{\sin \theta}{\sqrt{2}} \hat{\varepsilon}_{\parallel} + \left(\sin \phi_p \cos \theta + \frac{\cos \phi_p \sin \theta}{\sqrt{2}} \right) \hat{\varepsilon}_{\perp} \right] \quad (13)$$

where $\hat{\varepsilon}_{\parallel} = \hat{z}$ is a unit vector in the direction of z-axis, and $\hat{\varepsilon}_{\perp} = -\sin \phi_p \hat{x} + \cos \phi_p \hat{y} = \hat{\varepsilon}_{\parallel} \times \hat{k}$ is a unit vector which is orthogonal to both $\hat{\varepsilon}_{\parallel}$ and \hat{k} .

Using Eqs. (10) and (12), the argument of exponential in Eq. (9) can be written as

$$\omega \left(t - \frac{\hat{k} \cdot \mathbf{r}}{c} \right) = \omega \left[t - \frac{R}{c} \left(\cos \phi_p \sin \theta + \frac{\sin \phi_p \cos \theta}{\sqrt{2}} \right) \right]. \quad (14)$$

Since R is close to the radius of curvature of particle trajectory, θ can be replaced by $c\beta t/R$. Due to the relativistic beaming only for small values of ϕ_p will there be an appreciable radiation, and therefore the duration of pulse $\Delta t \sim R/c\gamma$ becomes very short. Hence the arguments of sine and cosine functions in Eqs. (13) and (14) are of the order of $1/\gamma$. So, we obtain

$$\hat{k} \times (\hat{k} \times \boldsymbol{\beta}) \approx \beta \left[\frac{\beta c}{\sqrt{2}R} t \hat{\varepsilon}_{\parallel} + \left\{ \frac{\beta c}{\sqrt{2}R} t + \phi_p \left(1 - \frac{c^2 \beta^2}{2R^2} t^2 \right) \right\} \hat{\varepsilon}_{\perp} \right] \quad (15)$$

and

$$\omega \left(t - \frac{\hat{k} \cdot \mathbf{r}}{c} \right) \approx \frac{\omega}{2} \left[\left(\frac{1}{\gamma^2} + \phi_p^2 \right) t + \frac{c^2}{3R^2} t^3 \right], \quad (16)$$

where β has been set equal to unity at wherever possible, and neglected all those terms which are of the order of $1/\gamma^2$ times those kept.

The components of electric field (Eq. 9) in the direction of unit vectors $\hat{\varepsilon}_{\parallel}$ and $\hat{\varepsilon}_{\perp}$ are:

$$E_{\parallel}(\omega) = -i \frac{q\beta^2 \omega}{2\sqrt{\pi} S_o R} e^{i\omega S_o/c} \int_{-\infty}^{+\infty} t \exp \left[i \frac{\omega}{2} \left\{ \left(\frac{1}{\gamma^2} + \phi_p^2 \right) t + \frac{c^2}{3R^2} t^3 \right\} \right] dt, \quad (17)$$

$$E_{\perp}(\omega) = -i \frac{q\beta \omega}{\sqrt{2\pi} S_o c} e^{i\omega S_o/c} \int_{-\infty}^{+\infty} \left\{ \frac{c\beta}{\sqrt{2}R} t + \phi_p \left(1 - \frac{c^2 \beta^2}{2R^2} t^2 \right) \right\} \exp \left[i \frac{\omega}{2} \left\{ \left(\frac{1}{\gamma^2} + \phi_p^2 \right) t + \frac{c^2}{3R^2} t^3 \right\} \right] dt. \quad (18)$$

To reduce the integrals into some known forms, we change the variable to

$$y = \left(\frac{1}{\gamma^2} + \phi_p^2 \right)^{-1/2} \frac{ct}{R} \quad (19)$$

and introduce a parameter

$$\xi_p = \frac{\omega R}{3c} \left(\frac{1}{\gamma^2} + \phi_p^2 \right)^{3/2}. \quad (20)$$

Therefore, the integrals are

$$I_1 = \frac{R}{c} \left(\frac{1}{\gamma^2} + \phi_p^2 \right)^{1/2} \int_{-\infty}^{+\infty} \exp \left\{ i \frac{3}{2} \xi_p \left(y + \frac{y^3}{3} \right) \right\} dy, \quad (21)$$

$$I_2 = \frac{R^2}{c^2} \left(\frac{1}{\gamma^2} + \phi_p^2 \right) \int_{-\infty}^{+\infty} y \exp \left\{ i \frac{3}{2} \xi_p \left(y + \frac{y^3}{3} \right) \right\} dy, \quad (22)$$

$$I_3 = \frac{R^3}{c^3} \left(\frac{1}{\gamma^2} + \phi_p^2 \right)^{3/2} \int_{-\infty}^{+\infty} y^2 \exp \left\{ i \frac{3}{2} \xi_p \left(y + \frac{y^3}{3} \right) \right\} dy. \quad (23)$$

We can identify these integrals with Airy integrals, and obtain the solutions:

$$I_1 = \frac{2}{\sqrt{3}} \frac{R}{c} \left(\frac{1}{\gamma^2} + \phi_p^2 \right)^{1/2} K_{1/3}(\xi_p), \quad (24)$$

$$I_2 = i \frac{2}{\sqrt{3}} \frac{R^2}{c^2} \left(\frac{1}{\gamma^2} + \phi_p^2 \right) K_{2/3}(\xi_p), \quad (25)$$

$$I_3 = -\frac{2}{\sqrt{3}} \frac{R^3}{c^3} \left(\frac{1}{\gamma^2} + \phi_p^2 \right)^{3/2} K_{1/3}(\xi_p), \quad (26)$$

where $K_{1/3}$ and $K_{2/3}$ are modified Bessel functions. Substituting the solutions of integrals into Eqs. (17) and (18), we get

$$E_{\parallel p}(\omega) = \frac{q\beta^2\omega R}{\sqrt{3\pi c^2 S_o}} e^{i\omega S_o/c} \left(\frac{1}{\gamma^2} + \phi_p^2 \right) K_{2/3}(\xi_p), \quad (27)$$

$$E_{\perp p}(\omega) = \sqrt{\frac{2}{3\pi}} \frac{q\beta\omega R}{c^2 S_o} e^{i\omega S_o/c} \left[\frac{\beta}{\sqrt{2}} \left(\frac{1}{\gamma^2} + \phi_p^2 \right) K_{2/3}(\xi_p) - i\phi_p \left(\frac{1}{\gamma^2} + \phi_p^2 \right)^{1/2} \left\{ 1 + \frac{\beta^2}{2} \left(\frac{1}{\gamma^2} + \phi_p^2 \right) \right\} K_{1/3}(\xi_p) \right], \quad (28)$$

where we have introduced a suffix 'p' on E_{\parallel} and E_{\perp} to indicate that they are due to a positron.

3.2. Radiation field due to an electron

For an electron, the position and velocity can be taken as

$$\mathbf{r}(t) = R \left(\sin \theta, -\frac{\cos \theta}{\sqrt{2}}, \frac{\cos \theta}{\sqrt{2}} \right), \quad (29)$$

$$\boldsymbol{\beta}(t) = \beta \left(\cos \theta, \frac{\sin \theta}{\sqrt{2}}, -\frac{\sin \theta}{\sqrt{2}} \right). \quad (30)$$

We choose the propagation vector for electron field as

$$\hat{\mathbf{k}} = (\cos \phi_e, \sin \phi_e, 0) \quad (31)$$

such that it is parallel to the $\hat{\mathbf{k}}$ in Eq. (12) and observer receives the radiation from both particles (positron-electron). Here ϕ_e is the angle between $\hat{\mathbf{k}}$ and the electron velocity. Using Eqs. (30) and (31), the vector part of the integrand in Eq. (9) can be written as

$$\hat{\mathbf{k}} \times (\hat{\mathbf{k}} \times \boldsymbol{\beta}) = \beta \left[\frac{\sin \theta}{\sqrt{2}} \hat{\boldsymbol{\varepsilon}}_{\parallel} + \left(\sin \phi_e \cos \theta - \frac{\cos \phi_e \sin \theta}{\sqrt{2}} \right) \hat{\boldsymbol{\varepsilon}}_{\perp} \right] \quad (32)$$

where $\hat{\boldsymbol{\varepsilon}}_{\parallel} = \hat{\mathbf{z}}$ and $\hat{\boldsymbol{\varepsilon}}_{\perp} = -\sin \phi_e \hat{\mathbf{x}} + \cos \phi_e \hat{\mathbf{y}} = \hat{\boldsymbol{\varepsilon}}_{\parallel} \times \hat{\mathbf{k}}$.

The argument of the exponential in Eq. (9) is

$$\omega \left(t - \frac{\hat{\mathbf{k}} \cdot \mathbf{r}}{c} \right) = \omega \left[t - \frac{R}{c} \left(\cos \phi_e \sin \theta - \frac{\sin \phi_e \cos \theta}{\sqrt{2}} \right) \right]. \quad (33)$$

Using the identical approximations and solutions of integrals used in the previous section for a positron field, we find the components of an electron field:

$$E_{\parallel e}(\omega) = \frac{1}{\sqrt{3\pi}} \frac{q\beta^2\omega R}{c^2 S_o} e^{i\omega S_o/c} \left(\frac{1}{\gamma^2} + \phi_e^2 \right) K_{2/3}(\xi_e), \quad (34)$$

$$E_{\perp e}(\omega) = -\sqrt{\frac{2}{3\pi}} \frac{q\beta\omega R}{c^2 S_o} e^{i\omega S_o/c} \left[\frac{\beta}{\sqrt{2}} \left(\frac{1}{\gamma^2} + \phi_e^2 \right) K_{2/3}(\xi_e) + i\phi_e \left(\frac{1}{\gamma^2} + \phi_e^2 \right)^{1/2} \left\{ 1 + \frac{\beta^2}{2} \left(\frac{1}{\gamma^2} + \phi_e^2 \right) \right\} K_{1/3}(\xi_e) \right]. \quad (35)$$

4. Polarization of radiation emitted by positrons and electrons

The electric fields $\mathbf{E}_p(\omega)$ and $\mathbf{E}_e(\omega)$ derived in Sect. 3 describe the polarization properties of OPM. It is clear that one mode is emitted by positrons and other by electrons. If the two radiation fields do not bear any phase relation then they are expected to be incoherently superposed at the observation point. On the other hand, if there is a phase relation then they are coherently superposed. From the observational point of view both the cases are important, and we discuss them separately in the following two subsections.

4.1. Incoherent superposition of radiation fields

Consider a region in the magnetosphere containing a large number of radiating positrons and electrons. Let each particle emit a pulse of radiation with electric field $\mathbf{E}_o(t)$. An

observer will detect a series of such pulses, all with same shape but random arrival times $t_1, t_2, t_3, \dots, t_N$. Then the measured electric field will be (Rybicki & Lightman 1979)

$$\mathbf{E}(t) = \sum_{j=1}^N \mathbf{E}_o(t - t_j), \quad (36)$$

where N is the number of particles. Taking the Fourier transform, we find

$$\mathbf{E}(\omega) = \frac{1}{\sqrt{2\pi}} \sum_{j=1}^N \int_{-\infty}^{+\infty} \mathbf{E}_o(t - t_j) e^{i\omega t} dt. \quad (37)$$

Let $u = t - t_j$ then $du = dt$. Therefore, we get

$$\mathbf{E}(\omega) = \mathbf{E}_o(\omega) \sum_{j=1}^N e^{i\omega t_j}. \quad (38)$$

Let dW , dA and $d\omega$ be the differential increments in energy, area and frequency, respectively. Then the measured spectrum is given by

$$\begin{aligned} \frac{dW}{dAd\omega} &= c|\mathbf{E}(\omega)|^2 \\ &= c|\mathbf{E}_o(\omega)|^2 \sum_{j=1}^N \sum_{k=1}^N e^{i\omega(t_j - t_k)} \\ &= c|\mathbf{E}_o(\omega)|^2 \left[N + \sum_{j \neq k}^N \cos \omega(t_j - t_k) \right]. \end{aligned} \quad (39)$$

Since t_j and t_k are randomly distributed in the case of radiation fields which do not have any phase relations, the second term averages to zero. Therefore, we have

$$\frac{dW}{dAd\omega} = c|\mathbf{E}(\omega)|^2 = Nc|\mathbf{E}_o(\omega)|^2. \quad (40)$$

Hence in an incoherent superposition of radiation fields the measured intensity will be simply a sum of intensities radiated by the individual charges.

4.2. Coherent superposition of radiation fields

The very high brightness temperature (10^{25} – 10^{30} K) of pulsars, lead to the conclusion that the radiation must be coherent. Pacini & Rees (1970), and Sturrock (1971) among others were quick to point out that the observed coherence may be due to bunching of particles in the emission region of magnetosphere. However, the topic of bunching mechanism continues to be an outstanding challenge. If the bunches of plasma particles with sizes much smaller than a wavelength exist then the arrival times $t_j \approx 0$, because all the pulses will have a same arrival time to order (size of bunch)/(wavelength). Then Eq. (38) gives

$$\mathbf{E}(\omega) \approx N\mathbf{E}_o(\omega). \quad (41)$$

Hence the total radiation field due to a bunch of particles is equal to the vector sum of the fields radiated by each charge.

Now, the measured spectrum is given by

$$\frac{dW}{dAd\omega} = c|\mathbf{E}(\omega)|^2 = N^2c|\mathbf{E}_o(\omega)|^2. \quad (42)$$

Hence the coherent sum of radiation fields of a bunch of particles leads to the intensity, which is equal to N^2 times the intensities due to the individual charges.

Since the pair creation, breakdown of polar gaps and sparks are not steady state processes, the plasma in the bunches can be neutral or nonneutral at an arbitrary time. If the bunches consist of prominently positrons (electrons) then the radiation field will be a coherent sum of \mathbf{E}_p of each positron (\mathbf{E}_e of each electron). In such cases, the two radiation fields are orthogonally polarized, and the modes are said to exist disjointly. On the other hand, if bunches are neutral then both charges can contribute equally and simultaneously to the radiation field. Since both the modes are coherently superposed in this case, we call this case joint. On the basis of individual pulse polarization Stinebring et al. (1984a) have concluded that OPM are superposed. If OPM exist disjointly their polarization properties are well defined, but not when they exist jointly. In the following two subsections we consider these cases in detail.

4.3. Presence of OPM disjointly

The OPM are said to exist disjointly when only one mode exists or one mode has become very strong compared to other mode. In all such cases the polarization state is solely determined by the stronger mode. The polarization state of OPM can be described more accurately using the Stokes parameters:

$$\begin{aligned} I_i &= E_{\parallel i} E_{\parallel i}^* + E_{\perp i} E_{\perp i}^* \\ &= \alpha^2 \left[\beta^2 \left(\frac{1}{\gamma^2} + \phi_i^2 \right)^2 K_{2/3}^2(\xi_i) + \phi_i^2 \left(\frac{1}{\gamma^2} + \phi_i^2 \right) \right. \\ &\quad \left. \times \left\{ 1 + \frac{\beta^2}{2} \left(\frac{1}{\gamma^2} + \phi_i^2 \right) \right\}^2 K_{1/3}^2(\xi_i) \right], \end{aligned} \quad (43)$$

$$\begin{aligned} Q_i &= E_{\parallel i} E_{\parallel i}^* - E_{\perp i} E_{\perp i}^* \\ &= -\alpha^2 \phi_i^2 \left(\frac{1}{\gamma^2} + \phi_i^2 \right) \left\{ 1 + \frac{\beta^2}{2} \left(\frac{1}{\gamma^2} + \phi_i^2 \right) \right\}^2 K_{1/3}^2(\xi_i), \end{aligned} \quad (44)$$

$$\begin{aligned} U_i &= 2\text{Re}[E_{\parallel i}^* E_{\perp i}] \\ &= \eta \alpha^2 \beta^2 \left(\frac{1}{\gamma^2} + \phi_i^2 \right)^2 K_{2/3}^2(\xi_i), \end{aligned} \quad (45)$$

$$\begin{aligned}
V_i &= 2\text{Im}[E_{\parallel i}^* E_{\perp i}] \\
&= -\sqrt{2}\alpha^2\beta\phi_i \left(\frac{1}{\gamma^2} + \phi_i^2\right)^{3/2} \left\{1 + \frac{\beta^2}{2} \left(\frac{1}{\gamma^2} + \phi_i^2\right)\right\} \\
&\quad \times K_{1/3}(\xi_i)K_{2/3}(\xi_i), \tag{46}
\end{aligned}$$

where

$$\xi_i = \frac{\omega R}{3c} \left(\frac{1}{\gamma^2} + \phi_i^2\right)^{3/2}, \quad \alpha = \sqrt{\frac{2}{3\pi}} \frac{q\beta\omega R}{c^2 S_o},$$

$i = p$ and $\eta = +1$ for positrons, and $i = e$ and $\eta = -1$ for electrons. The intensity and polarization angle of the linearly polarized radiation are:

$$L_i = \sqrt{U_i^2 + Q_i^2}, \tag{47}$$

$$\psi_i = \frac{1}{2} \tan^{-1} \left(\frac{U_i}{Q_i}\right). \tag{48}$$

Due to the action of forces \mathbf{F}_{Bi} and \mathbf{F}_{ci} , particle orbital planes become inclined with respect to the plane of magnetic field line. The radiation beams of the two charges appear on either sides of the plane of magnetic field line. Therefore, we define $\phi_p = \phi - \frac{1}{\gamma}$ and $\phi_e = \phi + \frac{1}{\gamma}$, where ϕ is the angle between the plane of magnetic field line and \hat{k} . Using $\gamma = 300$, $\nu = 1$ GHz and $R = 10^6$ cm, we computed the polarization parameters I_i , L_i , V_i and ψ_i , and plotted as functions of ϕ in Fig. 4. The continuous line curves describe the positron radiation field while the broken line curves for an electron radiation field. About the particle orbital planes, i.e., about $\phi_p = 0$ and $\phi_e = 0$, intensity and linear polarization have maxima while circular polarization undergoes sense reversal. Therefore, when observed with line-of-sight lying in the range $-\frac{1}{\gamma} < \phi < \frac{1}{\gamma}$ as indicated by a two way arrow in Fig. 4(c), one mode becomes right hand circularly polarized ($V_p > 0$) while the other becomes left hand circularly polarized ($V_e < 0$). Individual pulses from PSR B2020+28 (Cordes et al. 1978) and PSR B0950+08 (Fig. 10g) indicate OPM tend to have opposite circular polarization. Figure 4(d) shows the polarization angle as a function of ϕ , clearly, two modes are orthogonally polarized when I_i and L_i are in maxima. Since particles are constrained to follow the curved field lines, the polarization angle of each mode swings in accordance with the RVM. In the case of PSR B0329+54 at 408 MHz, Gil & Lyne (1995) have clearly shown that each of these modes is well described by the RVM.

The Stokes parameters of $\mathbf{E}_p(\omega)$ and $\mathbf{E}_e(\omega)$ clearly indicate OPM are elliptically polarized. The radiation field \mathbf{E}_p is polarized with $\sim 45^\circ$ while \mathbf{E}_e with $\sim -45^\circ$ with respect to the plane of magnetic field line. Figure 5 illustrates the polarization ellipses of OPM in the coordinate system with axes along the unit vectors $\hat{\epsilon}_{\parallel}$, $\hat{\epsilon}_{\perp}$ and \hat{k} , where the unit vector $\hat{\epsilon}_{\parallel}$ is parallel to the radius of curvature (ρ) of magnetic field line.

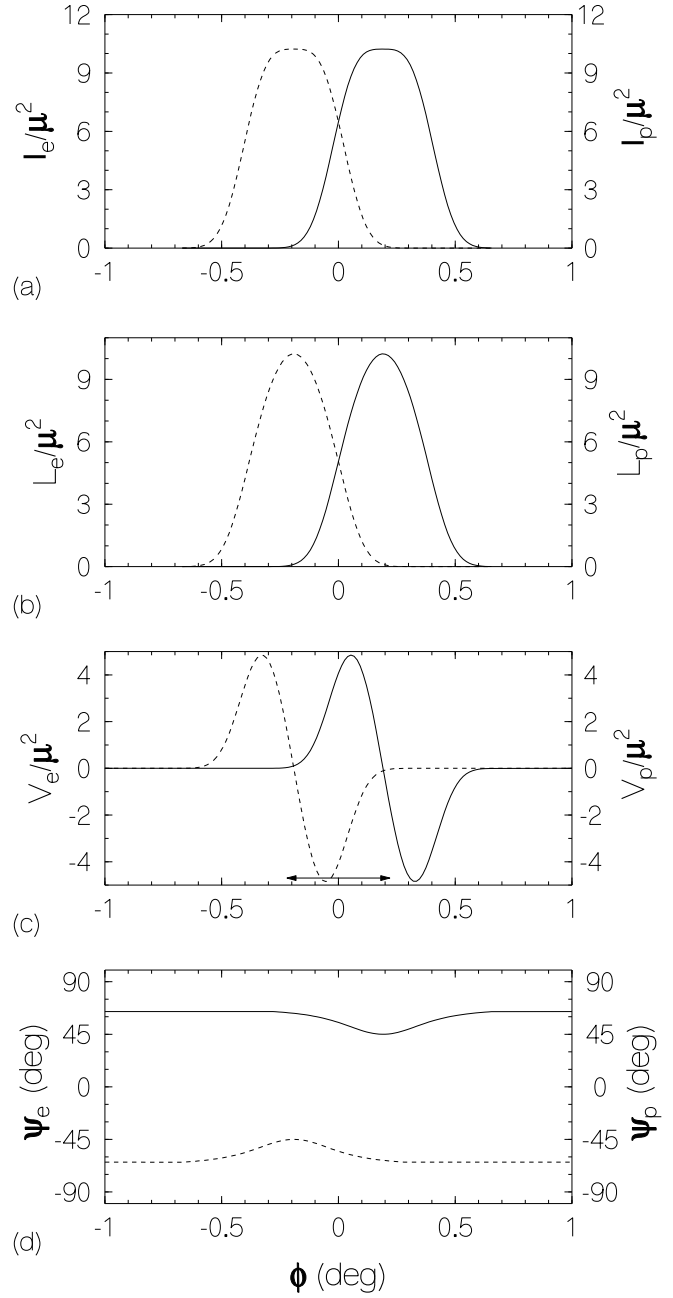


Fig. 4. Polarization parameters versus ϕ for the radiation due to a positron (continuous line curves) and an electron (broken line curves). The labels on vertical axes of panels (a), (b) and (c) are dimensionless as we have normalized with $\mu^2 = [q\beta^2\omega R/(3\pi)^{1/2}c^2 S_o\gamma^2]^2$.

As mentioned in Sect. 4.2, particle generation processes such as direct emission of electrons from the stellar surface due to the building up of high potential difference at the polar cap and the pair creation are not steady processes. They operate on time scales less than microseconds, therefore, the plasma which flows along the field lines is not always neutral. On time scales such as sampling time, it may look either negative or positive. In all such cases, the observer receives OPM at $\sim \pm 45^\circ$, depend-

ing upon the sign of plasma which exist at that particular instant. One mode is not radiated even when the plasma is neutral, if the energy of one kind of charge happens to fall below the threshold to radiate.

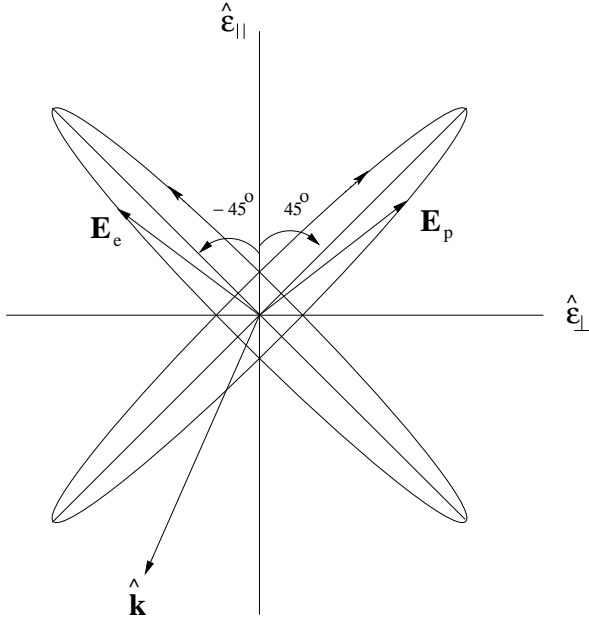


Fig. 5. Representation of OPM in a coordinate system with axes parallel to the orthogonal unit vectors $\hat{\epsilon}_{\parallel}$, $\hat{\epsilon}_{\perp}$ and \hat{k} , where $\hat{\epsilon}_{\parallel}$ is parallel to the radius of curvature (ρ) of magnetic field line.

4.4. Presence of OPM jointly

If the charges are close enough to each other (e.g. bunch), we may expect the fluctuations in amplitudes and phases of radiation fields will not be independent at the observation point. In the limit where the distance between the two charges is much less than a wavelength, the amplitudes vary in phase (Born & Wolf 1986). Therefore, when the Fourier components $\mathbf{E}_p(\omega)$ and $\mathbf{E}_e(\omega)$ are coherently superposed, we get

$$\mathbf{E}(\omega) = \mathbf{E}_p(\omega) + \mathbf{E}_e(\omega). \quad (49)$$

The Stokes parameters of total field can be defined similar to those (Eqs. 43–46) for OPM. Again using $\gamma = 300$, $\nu = 1$ GHz and $R = 10^6$ cm, we computed polarization parameters I , L , V and ψ of $\mathbf{E}(\omega)$, and plotted as functions of ϕ in Fig. 6. The two humps at $\phi \sim 0.2^\circ$ and -0.2° in Figs. 6(a) and (b) are due to the dominance of emission from positrons and electrons at those angles, respectively. Figure 6(c) shows the sense reversal of circular polarization about $\phi = 0$, i.e., about the plane of magnetic field line. The polarization angle of $\mathbf{E}(\omega)$ is plotted in Fig. 6(d), and the swing arises due to the coherent superposition of

OPM. This type of polarization angle swings are quite evident in micropulses and subpulses.

Consider a coordinate system-xyz such that the major axes of polarization ellipses of $\mathbf{E}_p(t)$ and $\mathbf{E}_e(t)$ are parallel to the axes x and y, respectively, as shown in Fig. 7. For the sake of illustration of OPM we represent them as

$$\mathbf{E}_p(t) = E_{xp} \cos(\omega t + \delta_p) \hat{x} + E_{yp} \sin(\omega t + \delta_p) \hat{y}, \quad (50)$$

$$\mathbf{E}_e(t) = E_{xe} \sin(\omega t + \delta_e) \hat{x} + E_{ye} \cos(\omega t + \delta_e) \hat{y}, \quad (51)$$

where E_{xi} , E_{yi} and δ_i are the amplitudes and initial phases. The period of rotation of electric fields is $T = 1/\nu$. For $\nu = 1$ GHz we find $T = 10^{-9}$ s, much smaller than the sampling interval in a typical observation ($\geq 1\mu\text{s}$).

Let $\delta = \delta_p - \delta_e$ be the phase difference between OPM, and ψ be the polarization angle of total field $\mathbf{E}(t)$ measured counter-clockwise from the x-axis. In Fig. 7, the ellipse drawn with dots indicate the polarization state of $\mathbf{E}(t)$ with the sense of rotation can be clockwise or counterclockwise or even nil, depending upon strengths of circular polarization of OPM. For the values of δ in the range $-\frac{\pi}{2}$ to $\frac{\pi}{2}$ we find ψ lies between 0 and $\frac{\pi}{2}$. On the other hand for values of δ in the range $\frac{\pi}{2}$ to $\frac{3\pi}{2}$, ψ takes values between $\frac{\pi}{2}$ and π . The polarization state of $\mathbf{E}(t)$ follows closely the stronger mode.

It is probable that separate streams of positrons and electrons exist in the pulsar magnetosphere (Sturrock, 1971). The mode changing observed in PSR B0329+54 by Hesse et al. (1973) indicate the channeling of particles along field lines is not steady. Assume that there exist two separate and closely spaced streams: one consists of mainly positrons and other electrons at longitudes ϕ_1 and ϕ_2 , respectively. When the observer's line-of-sight moves from ϕ_1 to ϕ_2 there will be an orthogonal *jump* in the polarization angle. Now, what happens to degree of polarization during those jumps? Let δt be the temporal separation between ϕ_1 and ϕ_2 . When one approaches ϕ_2 starting from ϕ_1 , field \mathbf{E}_p becomes progressively weaker while \mathbf{E}_e gets stronger. To find the polarization angle distribution during δt , let us divide the interval δt into n subintervals having the widths equal to the period ($T = 1/\nu$) of rotation of $\mathbf{E}(t)$. If δ lies between $-\frac{\pi}{2}$ and $\frac{\pi}{2}$ then $\mathbf{E}(t)$ will have ellipses $t_1 = T$, $t_2 = 2T$, ..., $t_n = nT = \delta t$ with polarization angles $\psi_1, \psi_2, \dots, \psi_n$, respectively, as shown in Fig. 8. On the other hand when δ lies between $\frac{\pi}{2}$ and $\frac{3\pi}{2}$ we get the ellipses $\tau_1 = T$, $\tau_2 = 2T$, ..., $\tau_n = nT = \delta t$ with polarization angles $-\psi_1, -\psi_2, \dots, -\psi_n$. If the observations are made with the time resolution, which is of the order of δt , we get total depolarization. This is because during the integration the electric fields oriented in all directions (dotted line ellipses) are superposed. The general result of observation that the orthogonal polarization angle jumps are accompanied by percentage of polarization going to zero, are caused by such an effect. For example, see the pulses of PSR B1804–08 and PSR B1905+39 by Xilouris et al. (1991).

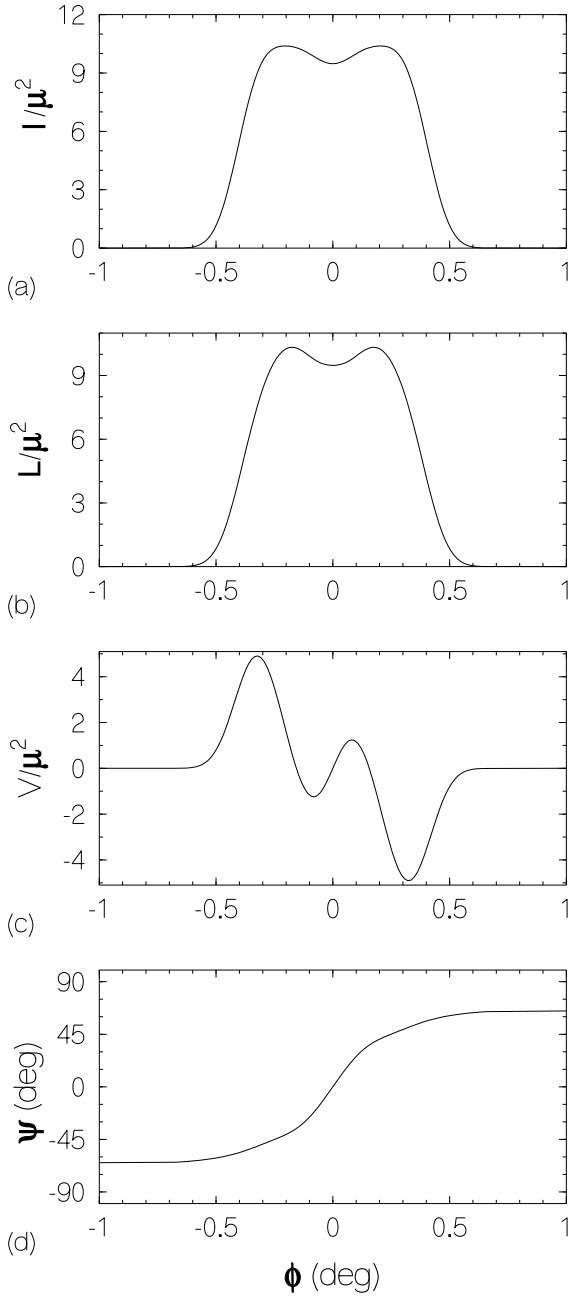


Fig. 6. Polarization parameters versus ϕ for the total radiation field $\mathbf{E}(\omega)$. The labels on vertical axes of panels (a), (b) and (c) are dimensionless as we have normalized with $\mu^2 = [q\beta^2\omega R/(3\pi)^{1/2}c^2S_0\gamma^2]^2$.

5. Discussion with an application to polarization of PSR B0950+08

In the previous sections we discussed the polarization properties of radiation emitted by positrons and electrons while moving along a curved magnetic field line. Here we extend our discussion to the emission from plasma streaming along many field lines. In the curved region of magnetic field lines, for the reasons given in Sect. 2, positrons move

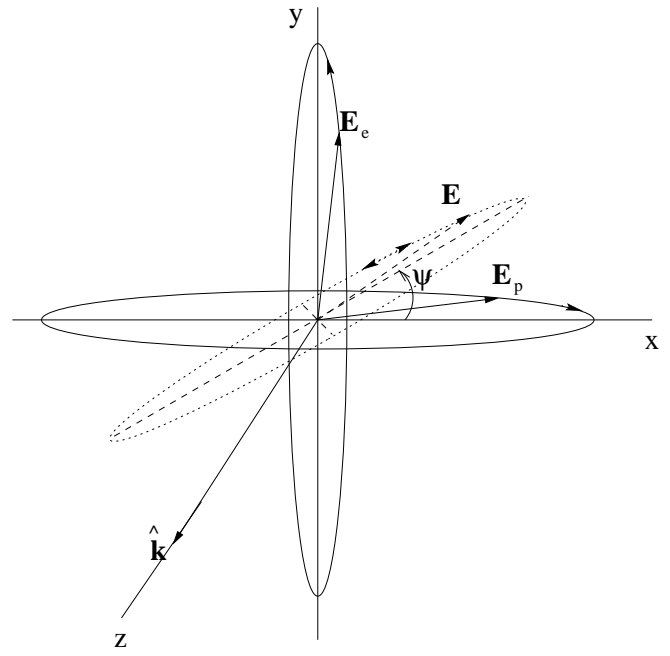


Fig. 7. Representation of OPM and total electric field $\mathbf{E}(t)$ in the coordinate system $-xyz$. The angle ψ represent the polarization angle of total field.

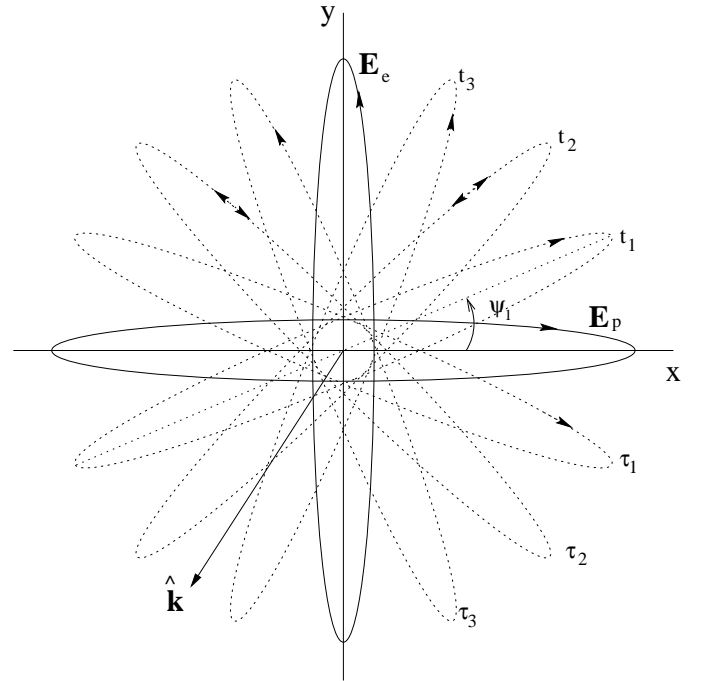


Fig. 8. Orthogonal polarization angle jumps occur when one mode say \mathbf{E}_p becomes weaker while the other mode \mathbf{E}_e gets stronger or vice versa over a small interval of pulse phase during pulsar rotation.

to one side of field line while electrons to other side as shown in Fig. 9. Let us consider three observing positions: A at the left side of the pulse, B at the middle and C at the right side.

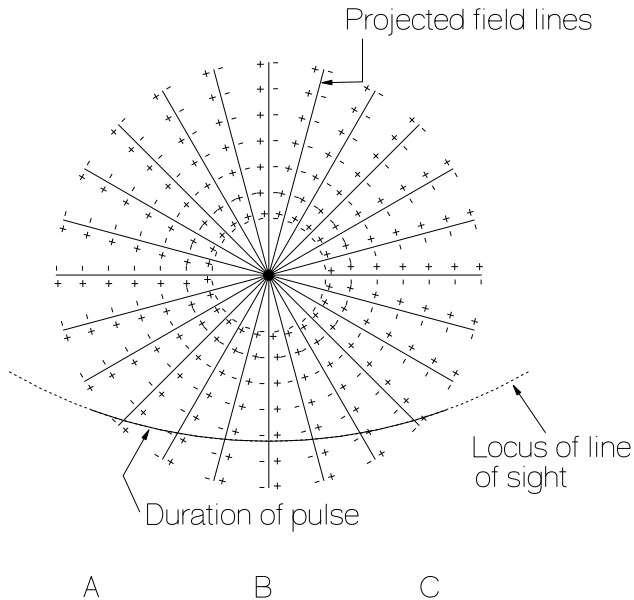


Fig. 9. Projected field lines loaded with positrons (+ signs) and electrons (- signs). Points A, B and C are the three observing positions.

At the position A, observer mainly receives radiation from the left side of planes of magnetic field lines, and the circular polarization of OPM tend show opposite senses (see Fig. 4c). An observer at position B (fiducial plane) views particle trajectory planes edge-on, therefore, the circular polarization of each mode undergoes sense reversal. Finally, an observer at C receives radiation mainly from the right side of planes of magnetic field lines, and circular polarization of each mode becomes opposite to its value in position A. If the OPM exist disjointly then the polarization angle of each mode swings in accordance with the RVM when the observers line-of-sight moves from point A to C.

Radhakrishnan & Rankin (1990) have identified the two extreme types of circular polarization signatures: an antisymmetric type (Fig. 6d) wherein the circular polarization changes sense at the middle of the pulse, and a symmetric type wherein it is predominantly of one sense. Our model can easily explain the antisymmetric type of circular polarization, while for symmetric type we need further analysis on the high resolution data of individual pulses.

5.1. Observations of PSR B0950+08

The pulsar PSR B0950+08 was observed in 1994 April by using the 100-m Effelsberg radiotelescope. Using a tunable HEMT-receiver with a system temperature of 28 K, observations were made at the center frequency of 1.71 GHz with a bandwidth of 40 MHz. The two circular polarizations are separated in the receiver and amplified. The signal is then fed into an adding polarimeter, a passive device with four output channels which allows further online signal processing. The pulse-smearing caused by the dispersion due to the interstellar medium is then removed using an online dedispersion device. This is a four unit 60×667 kHz filterbank. The output of each channel is then detected and converted into a digital signal by a fast A/D converter. After a time delay according to the dispersion measure, the outputs of all channels are added and then recorded by the backend. After a careful calibration procedure, Stokes parameters are obtained from the four recorded output channels. A detailed system description and the calibration procedure are given by von Hoensbroech & Xilouris (1997). At frequency 1.71 GHz, we recorded about 1200 pulses with a time resolution of 0.24 ms.

We consider only the main pulse as the interpulse is too weak to reproduce the properties of OPM. The average polarization parameters are plotted as functions of pulse phase ϕ in Fig. 10(a). The continuous line curve indicates intensity (I) variation while broken and dotted ones indicate linear (L) and circular (V) polarization, respectively, in arbitrary units.

The gray-plots show the frequency of occurrence of OPM at different pulse phases, and have become powerful tools in analyzing the pulsar polarization properties. The darkest regions represent the most probable regions of occurrence. For each pulse phase bin where I is above 3σ level of its value in the off pulse region, gray-plots were computed for L , V , I and polarization angle ψ . All those phase bins, where the condition $L^2 + V^2 \leq I^2$ was not met, were excluded as they lead to spurious interpretation of polarization. The points with error bars in Fig. 10(b) indicate the integrated polarization angle superposed over the polarization angle gray-plot. Figures 10(c)–(e) represent the gray-scale maps of percentage of linear polarization [$L(\%) = 100L/I$], circular polarization [$V(\%) = 100V/I$] and I , respectively, while Figs. 10(f)–(h) represent the gray-scale scatter plots of $L(\%)$, $V(\%)$ and I versus the polarization angle ψ .

The polarization angle gray-plot (Fig. 10b) shows the two most preferred tracks close to 45° and -45° position angles in the ψ versus ϕ plane, in agreement with our model (Fig. 4d). The frequency of occurrence of OPM with respect to the polarization angle is shown in Fig. 11, proving the importance of OPM in the pulsar radiation. At any pulse longitude the average polarization angle curve follows closely the mode which is more intense, as indi-

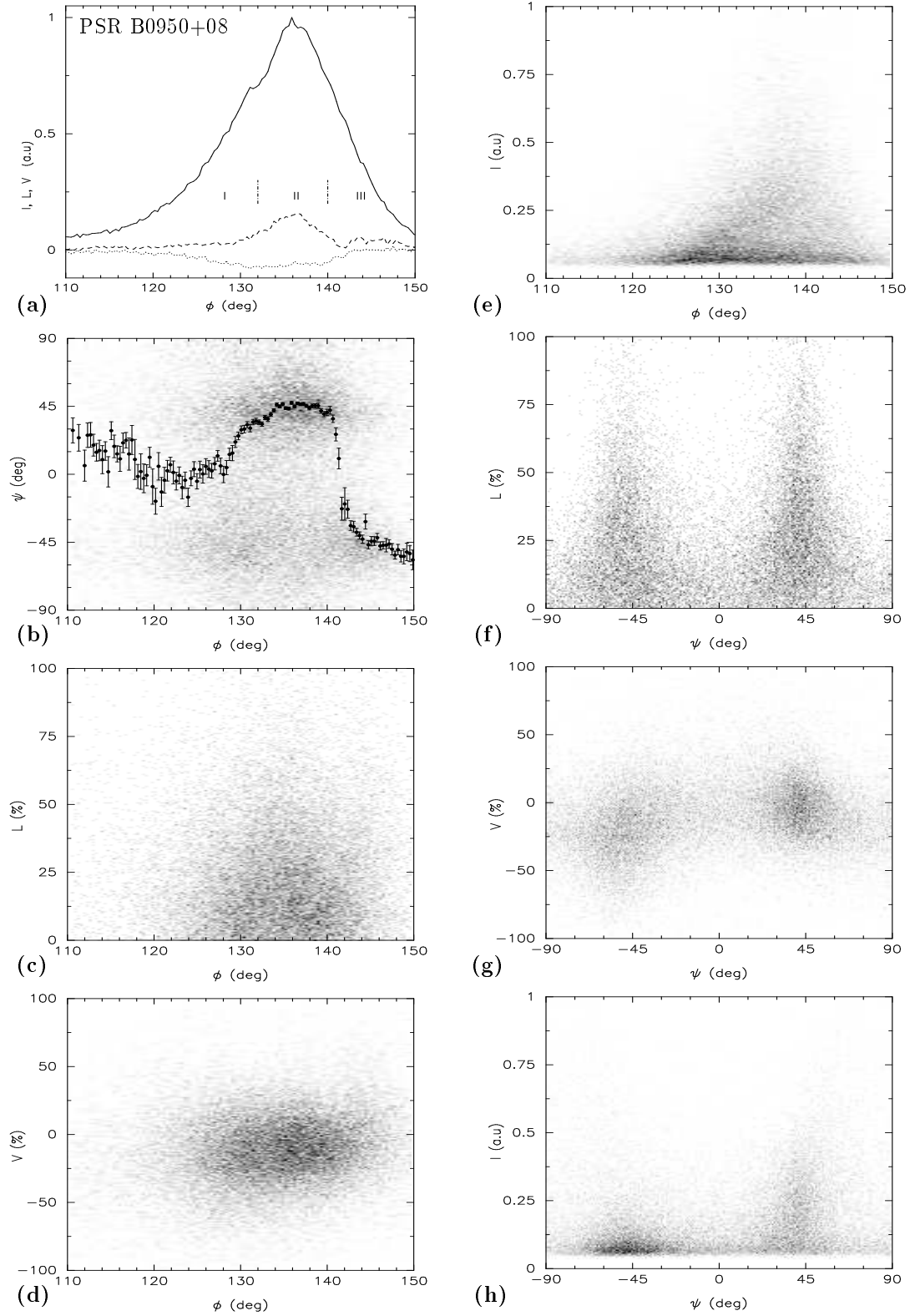


Fig. 10. Polarization histograms of pulsar PSR B0950+08 at frequency 1.71 GHz: (a) average pulse with arbitrary units (a.u), (b) polarization angle ψ , (c) & (f) percentage of linear polarization, (d) & (g) percentage of circular polarization, and (e) & (h) intensity. The angle ϕ denotes the pulse phase.

cated by Fig. 10(b). The uniform or random component of polarization angle is probably due to the coherent superposition of OPM (see Figs. 6d&7). This idea is also supported by the observation that the random component becomes significant only at those pulse longitudes where both modes exit. For example, see the polarization angle displays of PSR B0823+26, B0950+08 (Stinebring et al. 1984a), B0834+06 (Stinebring et al. 1984b), and B0329+54 (Gil & Lyne 1995). McKinnon and Stinebring (1996) have also suggested that the random component may arise from superposed modes. Barnard & Arons (1986) have proposed ω^{-2} frequency dependence for angular separation of OPM, but our model do not predict any appreciable frequency dependence.

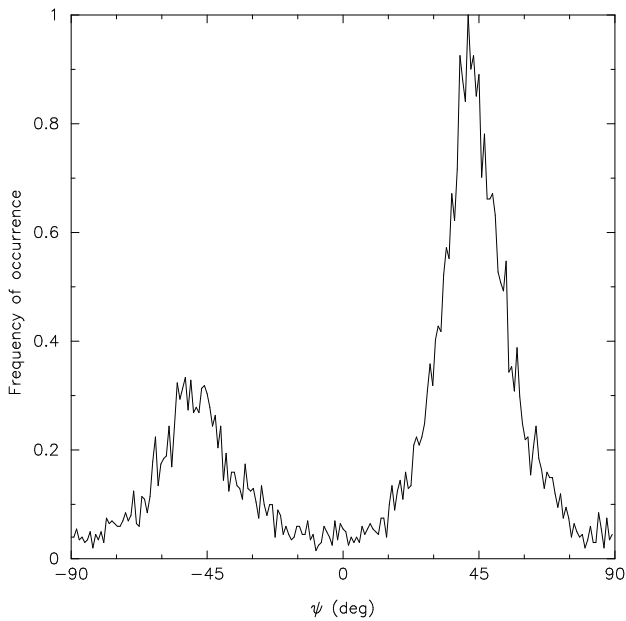


Fig. 11. Frequency of occurrence of pulses with respect to the polarization angle.

On the basis of relative frequency of occurrence of OPM at different pulse longitudes as indicated by Figs. 10(b), we may identify pulse longitude ranges I, II and III, as marked in Fig. 10(a). It is clear that both modes exist at all pulse longitudes but one mode dominates over the other at some longitudes. For example, in region II the mode (say mode 1) with $\psi \sim 45^\circ$ dominates while in region III the other mode (mode 2) with $\psi \sim -45^\circ$ dominates.

When the frequency of occurrence of OPM is very high as in region II, it is likely that more often they simultaneously exist. If so then they get superposed either coherently or incoherently depending upon whether there is any phase relation between them or not. Figure 10(d)

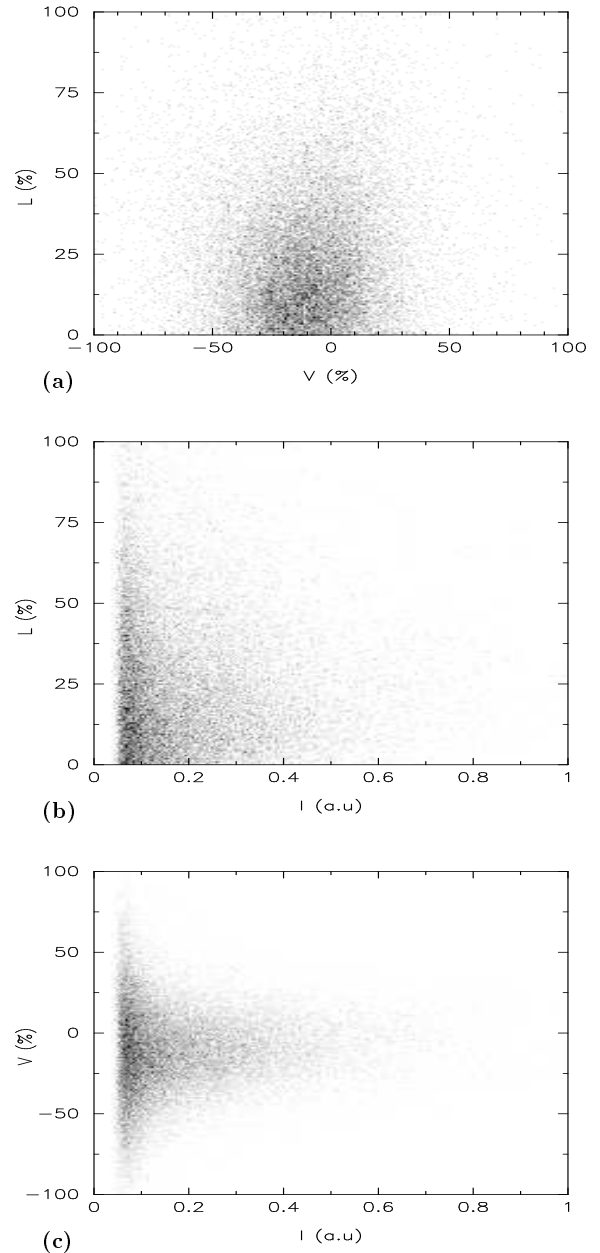


Fig. 12. Grey-scale plots representing the correlations between $L(\%)$, $V(\%)$ and I in the individual pulses.

shows, at any pulse longitude, circular polarization can be of either sense depending upon from which side of particle trajectory the radiation is received (see Fig. 4c). The distribution of different pulse intensities (arbitrary units) versus ϕ is shown in Fig. 10(e).

In revealing the properties of OPM, Figs. 10(f)–(h) are much more expressive than Figs. 10(c)–(d) as the earlier ones directly display the distributions against the polarization angle ψ . Figures 10(f) and (g) indicate that if the modes exist disjointly, they appear at $\sim \pm 45^\circ$ with

high linear and circular polarization, but the random component is less polarized. Figure 10(g) shows OPM tend have opposite circular polarization (see Fig. 4c&d). Figure 10(h) shows the distribution of intensities of OPM versus the polarization angle, and it indicates the mode 1 is stronger than the mode 2.

From the theoretical point of view, it is very important to find the correlations between $L(\%)$, $V(\%)$ and I . Using the individual pulse data, we computed the grey-plots (Fig. 12), which represent the correlations between different polarization parameters. Figure 12(a) shows *linear polarization becomes maximum when the circular polarization is at minimum*, a prediction of curvature radiation (see Figs. 4b&c).

The behaviour of $L(\%)$ with respect to I is shown in Fig. 12(b). It shows anticorrelation between I and $L(\%)$ at higher intensities. The sharp cutoffs close to the vertical axis is due to the condition that I is above 3σ level. Manchester et al. (1975) and Xilouris et al. (1994) have also indicated the anticorrelation between I and $L(\%)$. The behaviour of circular polarization with respect to the intensity is shown in Fig. 12(c). At higher intensities, circular polarization is lower. The reason could be the superposition of OPM with opposite senses of circular polarization.

6. Conclusion

The motion of particles along the curved field lines cannot be described in analogy with the motion of particles in a central force. The radiation emitted by positrons and electrons while moving along the curved magnetic field lines is probably orthogonally polarized. The radiation is highly polarized when the OPM are not superposed. The polarization angle of each mode swings in accordance with the RVM. However, the polarization angle swings observed in micropulses and subpulses are often found to be contrary to the predictions of RVM. We expect such swings are produced when the OPM are coherently superposed. Our model do not predict any appreciable frequency dependence on the angular separation between OPM. The circular polarization of OPM tend to have opposite senses.

The observations of PSR B0950+08, particularly, polarization angle, linear and circular polarizations of OPM are in agreement with our model. The polarization histograms clearly indicate that the depolarization is due to the superposition of OPM. This effect becomes much more severe at higher frequencies as the coherence-length which is of the order of wavelength becomes small leading to an incoherent superposition of OPM.

Acknowledgements. I would like to thank L. A. Nowakowski and K. Rozga for confirming the solutions of integrals, and A. v. Hoensbroech and M. Kramer for their help in reducing the data. It is a pleasure to thank D. Lorimer for his comments on the manuscript, and A. Jessner, A. G. Lyne, W. Kundt, G.

Smith and R. Wielebinski for several interesting and stimulating discussions. This work was supported by a fellowship of the Alexander-von-Humboldt foundation.

References

- Backer D.C., Rankin J.M., Campbell D.B. 1976, Nat. 263, 202
 Barnard J.J., Arons J., 1986, ApJ 302, 138
 Born M., Wolf E. 1986, Principles of Optics (New York: Pergamon), p. 491
 Cordes J.M. 1983, in Positron–Electron pairs in Astrophysics, ed. Burns M.L., Harding A.K., Ramaty R., AIP Conf. Proc. 101, 98
 Cordes J.M., Hankins T.H. 1977, ApJ 218, 484
 Cordes J.M., Rankin J.M., Backer D.C. 1978, ApJ 223, 961
 Gangadhara R.T. 1995, Ap&SS 232, 327
 Gangadhara R.T. 1996a, A&A 314, 853
 Gangadhara R.T. 1996b, IAU Colloquium 160: Pulsars: Problems & Progress, eds. S. Johnston, M. A. Walker & M. Bailes, ASP Conf. Seri. 105, 185
 Gil J.A., Lyne A.G. 1995, MNRAS 276, L55
 Gil J.A., Snakowski J.K. 1990, A&A 234, 237
 Good R.H., Müller E.W. 1956, Handbuch der Physik, 21, 1
 Herring C., Nicholas M.H. 1949, Rev. Mod. Phys. 21, 185
 Hesse K.H., Sieber W., Wielebinski R. 1973, Nat. 245, 57
 von Hoensbroech A., Xilouris X.M., 1997, A&A, in press
 Jackson J.D. 1976, Classical Electrodynamics, 2nd ed., Wiley, London
 Kundt W., Schaaf R., 1993, Ap&SS 193, 145
 Lyne A.G., Smith F.G., Graham D.A. 1971, MNRAS 153, 337
 Lyne A.G., Smith F.G. 1990, Pulsar Astronomy, Cambridge Univ. Press, Cambridge, p. 234
 Manchester R.N. 1971, ApJS 23, 283
 Manchester R.N., Taylor J.H., Huguenin G.R. 1975, ApJ 196, 83
 McKinnon M.M., Stinebring D.R., 1996, IAU Colloquium 160: Pulsars: Problems & Progress, eds. S. Johnston, M. A. Walker & M. Bailes, ASP Conf. Seri. 105, 483
 Melrose D.B. 1981, in Sieber W., Wielebinski R., eds, Pulsar, 13 years of Research on Neutron Stars. D. Reidel: Dordrecht, p. 133
 Mészáros P. 1992, High–Energy Radiation from Magnetized Neutron Stars (Chicago: Univ. Chicago Press)
 Michel F.C. 1987a, ApJ 322, 822
 Michel F.C. 1987b, Comments Ap. 12, 191
 Michel F.C. 1991, Theory of Neutron Star Magnetospheres, (Chicago: Univ. Chicago Press)
 Pacini F., Rees M.J. 1970, Nat. 226, 622
 Radhakrishnan V., Cooke D.J. 1969, Astrophys. Lett. 3, 225
 Radhakrishnan V., Rankin J.M. 1990, ApJ 352, 258
 Rankin J.M., Campbell D.B., Backer D.C. 1974 ApJ 188, 608
 Rybicki G.B., Lightman A.P. 1979, Radiative Processes in Astrophysics, A Wiley–Intersci. Pub., New York, p. 104
 Ruderman M., Sutherland P. 1975, ApJ 196, 51
 Stinebring D.R., et al. 1984a, ApJS 55, 247
 Stinebring D.R., et al. 1984b, ApJS 55, 279
 Sturrock P.A. 1971, ApJ 164, 529
 Xilouris K.M., Rankin J.M., Seiradakis J.H., Sieber W. 1991, A&A 241, 87
 Xilouris K.M., Kramer M., Jessner A., Wielebinski R. 1994, A&A 288, L17

This article was processed by the author using Springer-Verlag
L^AT_EX A&A style file *L-AA* version 3.